

Ratio-Preserving Ellipse-Fit Alignment for Robust 2-D Shape Recognition

Mehmet FIDAN^{1,*}, Semih ERGIN², Mehmet KOÇ³, Mehmet Bilginer
GÜLMEZOĞLU², Ömer Nezir GEREK⁴, and Atalay BARKANA⁴

¹Vocational School of Transportation, Eskisehir Technical University, Eskisehir, Turkey

²Department of Electrical and Electronics Engineering, Eskisehir Osmangazi University,
Eskisehir, Turkey

³Department of Computer Engineering, Eskisehir Technical University, Eskisehir, Turkey

⁴Department of Electrical and Electronics Engineering, Eskisehir Technical University,
Eskisehir, Turkey

Email: mfidan@eskisehir.edu.tr*, sergin@ogu.edu.tr,
mehmetkoc@eskisehir.edu.tr, bgulmez@ogu.edu.tr,
ongerek@eskisehir.edu.tr, atalaybarkana@eskisehir.edu.tr

* Corresponding author

Abstract. A lightweight yet powerful pipeline for 2-D shape recognition is presented, preserving each shape's intrinsic aspect ratio while aligning it to every reference candidate. The approach first fits ellipses to query and reference shapes, then rescales the query's minor axis so that its original major-to-minor ratio is kept unchanged after mapping to the reference ellipse. A single affine matrix obtained from the updated vertices compensates for translation, rotation, and global scale in one step. This work introduces a novel ratio-preserving ellipse-fit alignment (RPEF) technique that significantly enhances robustness in 2-D shape recognition, particularly under varying orientations and scales. Unlike traditional approaches such as the Randomized Hough Transform or HyperLS, which struggle with noisy data or iterative complexities, RPEF ensures numerical stability and efficiency by leveraging a geometrically informed prior. The approach's key contribution lies in its ability to maintain shape integrity without requiring extensive training data, making it highly adaptable for applications with limited labeled datasets, such as medical image analysis or industrial inspection. Additionally, the pipeline's one-step affine transformation simplifies the alignment process, outperforming existing approaches like LShape descriptors by achieving superior accuracy metrics, 100% on Kimia-99 and 85.5% on TARI-1000, demonstrating its practical utility and effectiveness in real-world scenarios.

Key-words: 2-D shape recognition; affine transformation; ellipse fitting; ratio-preserving scalings; similarity metrics.

1. Introduction

The recognition of binary shapes is a fundamental task in computer vision and pattern recognition. Early work explored Bayesian modeling of dynamic scenes [1], hierarchical shape-based object representation [2], Binary Partition Trees for shape detection [3], and similarity-based classification [4]. Shape representation has been studied with region-based approaches for content-based image acquisition [5], and the perception of shape features like curvature has been investigated [6].

Beyond computer-vision-specific studies, recent advances in nonlinear modelling and learning show the same principles at work in cognitive observation processes [7], in online semi-supervised ensemble fuzzy systems that handle streaming data with missing values [8], and in statistical computational models that explain the highly-nonlinear composition of nuclear-fuel fission products and their gas-aerosol emissions [9]. Complementary advances in data-driven classification show similar gains in recognition accuracy, such as a centroid-update variant of k-means clustering that accelerates convergence [10], and score-normalized fusion of online signatures and fingerprints that boosts multimodal biometric performance [11].

Ellipse fitting is a common challenge in shape analysis [12]. Ellipses represent perspective projections of circles and are used in 3D vision, object recognition, medical imaging, and industrial inspection [12]. Halir and Flusser developed a numerically stable least-squares algorithm for ellipse fitting, ensuring an ellipse-specific solution even with noisy data [12]. The Randomized Hough Transform (RHT) faces challenges with non-linear parameter equations in ellipse detection, though linearization approaches exist [13].

Ellipse fitting techniques have evolved over time. Early least-squares-based approaches from the 1970s were noise-sensitive. The 1990s introduced renormalization, improving robustness. The 2000s brought FNS and HEIV approaches, enhancing accuracy [14]. Later advancements like hyperaccurate correction (2006), HyperLS (2009), and hyper-renormalization (2012) improved efficiency and reduced bias [14]. Preprocessing techniques, such as multi-scale smoothing, handle outliers [15].

Shape similarity measures are crucial for image retrieval [16]. Machine learning approaches like biased maximum margin analysis have integrated features in SVM-based schemes [17]. Handling scaling and rotation variations remains a challenge. Matching algorithms, including hierarchical matching [18] and point matching [19], improve robustness. View-based approaches recognize 3D objects from 2D views [20]. Algorithms like the Kabsch algorithm calculate optimal rotation matrices [21], sometimes called partial Procrustes superimposition [22].

Recent deep learning approaches align shapes using incomplete data [23], symmetry properties [24], or point correspondences [25]. Shape alignment has been formulated as a linear programming problem [26]. Shape descriptors like L-Shaped patterns [27], quadratic Bezier triangles [28], and octagonal lattice-based descriptors [29] have been applied to datasets like Kimia and TARI.

The main contribution of this work is a novel ratio-preserving ellipse-fit alignment approach that enhances 2D shape recognition by maintaining geometric ratios during affine transformations, achieving superior classification performance on datasets like Kimia and TARI without the

need for training data. The proposed alignment improves shape-matching-based classification of binary images without requiring more complicated correlation-based preprocessing steps at each step of the classification. By training the ellipse parameters using a fraction of the data, the remaining test data could use the trained parametrization to achieve a successful alignment for shape matching.

Existing approaches such as AlignNet or point set registration often require extensive training data or are sensitive to rotation. Authors' approach provides a lightweight, training-free alternative that preserves intrinsic geometric properties, making it suitable for limited-data and variable-orientation scenarios.

Unlike recent approaches in 2D shape recognition, such as generalized Procrustes alignment [26], L-shaped geometry-based descriptors [27], and quadratic Bézier triangle-based approaches [28], the proposed ratio-preserving ellipse-fit alignment approach uniquely maintains geometric ratios during affine transformations, ensuring robust shape matching without distortion of intrinsic shape properties. While robust ellipse fitting techniques, such as those using Laplacian kernel [30] or hierarchical Gaussian mixture models, focus on handling noisy boundaries, they do not explicitly preserve geometric ratios, which is critical for accurate binary shape classification. Additionally, the approach proposed in this paper eliminates the need for complex correlation-based preprocessing steps, as seen in traditional pixel overlap approaches [31], and achieves computational efficiency with a complexity of $\mathcal{O}(N) + T\mathcal{O}(P)$, making it more practical for real-time applications compared to transformation decomposition approaches.

The paper is organized as follows: Section 2 reviews related literature, Section 3 introduces the proposed alignment framework, Section 4 reports experimental validation and performance analysis, Section 5 discusses results, limitations, and implications, and Section 6 concludes the paper by highlighting key contributions and future directions.

2. Related Work

To contextualize the approach, recent advancements in 2D shape recognition are reviewed. Approaches like L-Shaped geometry-based descriptors [27] and octagonal lattice-based triangulated shape descriptors [29] have improved retrieval accuracy on datasets like Kimia and TARI. Deep learning techniques, such as AlignNet [23], leverage unsupervised learning for partial shape alignment, while traditional approaches like the Kabsch algorithm [21] focus on point set registration. The ratio-preserving ellipse-fit approach offers improved invariance to scale and rotation without requiring training data.

These cross-domain contributions illustrate how nonlinear-model learning frameworks adapt to heterogeneous, noisy, or incomplete data: from cognition-inspired observation modelling [7] to the OSSEFS fuzzy-ensemble stream learner [8] and the rank-size statistical model of nuclear-emission spectra [9]. They motivate the emphasis on ratio preservation as a bias-free geometric prior. Recent studies further illustrate effective strategies that align with the objectives of the present work. The centroid-update approach improves the efficiency of k-means clustering while preserving cluster quality [10], and score-level fusion with prior normalization enhances recognition in multimodal biometric systems [11]. These insights reinforce the importance of robust distance metrics and normalization, motivating the ratio-preserving alignment scheme proposed in this study.

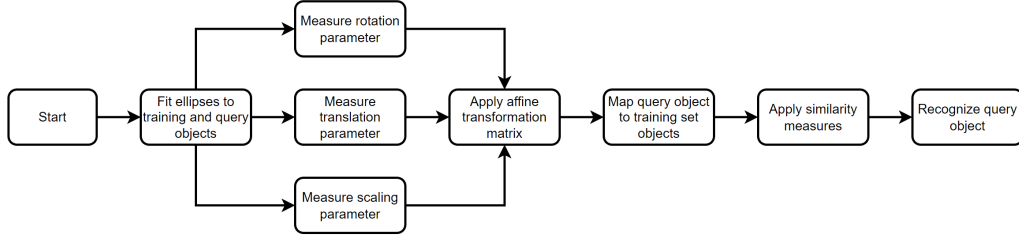


Fig. 1. Flowchart for alignment of the shapes and shape matching in 2D images.

3. Alignment of the Shapes and Shape Matching in 2D Images

3.1. Ellipse fit and ratio-preserving rescale

Ellipses are fitted to binary image objects in the Kimia and TARI databases using Matlab's `regionprops` function. To address rotation, translation, and scaling, an affine transformation matrix with homogeneous coordinates is created to map each test object onto its corresponding training object. Recognition is achieved by comparing the overlap between the transformed test and training objects. The flowchart is shown in Fig. 1.

Ratio-preserving rescale. Let the query ellipse have major axis L_Q , minor axis l_Q , and ratio $r_Q = L_Q/l_Q$. When aligning to a reference ellipse with major axis L_i , the minor axis is redefined as

$$l'_Q = \frac{L_i}{r_Q} = \frac{L_i l_Q}{L_Q}. \quad (1)$$

Eq. (1) is evaluated in the fourth line of Algorithm 1. Using the updated vertices, a single affine matrix is computed to map the query shape onto the reference shape. Algorithm 1 performs exactly the six numbered operations introduced in Sections 3.1–3.4.

A compact overview of every model parameter—and the exact equation or algorithm line that computes it—is given in Table 1 immediately following Algorithm 1.

Algorithm 1 Ratio-Preserving Ellipse-Fit Alignment and Matching

Require: query shape \mathbf{Q} ; training set $\mathcal{T} = \{\mathbf{T}_i\}_{i=1}^N$

Ensure: predicted class label \hat{y}

- 1: $(L_Q, l_Q, r_Q, V_Q) \leftarrow \text{FITELLIPSE}(\mathbf{Q})$ $\triangleright r_Q = L_Q/l_Q$
 - 2: **for** $i \leftarrow 1$ **to** N **do**
 - 3: $(L_i, l_i, r_i, V_i) \leftarrow \text{FITELLIPSE}(\mathbf{T}_i)$
 - 4: $l'_Q \leftarrow L_i/r_Q$ \triangleright ratio-preserving minor axis
 - 5: $V'_Q \leftarrow \text{UPDATEVERTICES}(V_Q, l'_Q)$
 - 6: $\mathbf{M}_i \leftarrow \text{AFFINEMATRIX}(V'_Q, V_i)$
 - 7: $\tilde{\mathbf{Q}}_i \leftarrow \mathbf{M}_i \mathbf{Q}$ \triangleright warp query
 - 8: $\mathbf{s}_i \leftarrow \text{SIMILARITYMETRICS}(\tilde{\mathbf{Q}}_i, \mathbf{T}_i)$
 - 9: **end for**
 - 10: $\hat{y} \leftarrow \text{MAJORITYVOTE}(\{\mathbf{s}_i\}_{i=1}^N)$
-

Table 1. Model components, symbols, and how each parameter is obtained. Section (§) and equation (Eq.) references point to the precise location of the computation in the text

Block	Parameter	Computation / reference	Dims
Ellipse fit	centroid, axes, orientation	regionprops (§3.1)	6 scalars
	L_Q, l_Q	returned by regionprops; see Alg. 1 L1	2 scalars
Rescale	$r_Q = L_Q/l_Q$	Definition; Alg. 1 L1	1 scalar
	$l'_Q = L_i/r_Q$	Eq. (1)	1 scalar
Affine align	$\mathbf{M} = [s\mathbf{R} \ t]$	Closed form $\mathbf{M} = \mathbf{CA}^{-1}$ (Eq. (6)) \rightarrow Alg. 1 L6–7	2×3
Overlap counts	TP, FP, TN, FN	Pixel conjunction / disjunction (§3.4) \rightarrow Alg. 1 L8	4 scalars
Metrics	ACC, F1, MCC, TS, BA, FM, BM, MK	Alg. 1 L8–9	8 scalars
Decision	\hat{y}	Majority of metric ranks \rightarrow Alg. 1 L10	1 label

3.2. Classification approach

The classification of 2D shapes in this paper follows a systematic pipeline that integrates ellipse fitting, ratio-preserving transformations, and pixel overlap metrics to achieve robust shape recognition. The steps of the classification approach, along with their interconnections, are outlined below:

1. **Ellipse Fitting:** An ellipse is fitted to each binary shape in the Kimia and TARI databases using least-squares optimization in MATLAB to approximate its boundary. This step, detailed in Section 3.1, establishes the geometric foundation for subsequent transformations.
2. **Ratio-Preserving Rescaling:** The fitted ellipse is rescaled to preserve its original major-to-minor axis ratio ($r_q = L_a/L_b$) while aligning it with a reference ellipse. This ensures that the shape’s intrinsic properties are maintained, providing a consistent basis for alignment (see Section 3.1).
3. **Affine Transformation:** An affine transformation matrix is computed using the rescaled ellipse to align the query shape with each reference shape in the training set. This step accounts for translation, rotation, and scaling, linking the rescaling output to the alignment process.
4. **Shape Alignment:** The query shape is transformed using the affine matrix, producing a set of aligned shapes corresponding to each reference shape. This alignment enables direct comparison by ensuring spatial correspondence.
5. **Pixel Overlap Calculation:** For each aligned shape pair, pixel overlap metrics (e.g., Accuracy Score, F1 Score) are computed to quantify similarity between the transformed query shape and reference shapes. This step builds on the alignment to measure shape similarity numerically.
6. **Classification Decision.** For each reference T_i , we compute the eight confusion-matrix-based similarity metrics $s_i = \{\text{ACC, F1, MCC, TS, BA, FM, BM, MK}\}$ from the overlap of \tilde{Q}_i and T_i . Each metric independently ranks the references; the query is then assigned the class label that wins a *majority vote* across the eight per-metric rankings (tie-break: highest ACC, then MCC, then TS).

3.3. Alignment of the shapes

The objective is to recognize 2D shapes by standardizing their analysis. Each shape's center is shifted to the origin, and an ellipse is fitted using least-squares [31], determining its major and minor axes [12, 13]. Vertices at the intersection of the axes with the ellipse are identified for geometric transformations addressing rotation, translation, scale variance, and shearing. The query shape is transformed onto each training set shape for matching, with the best match determining the class label.

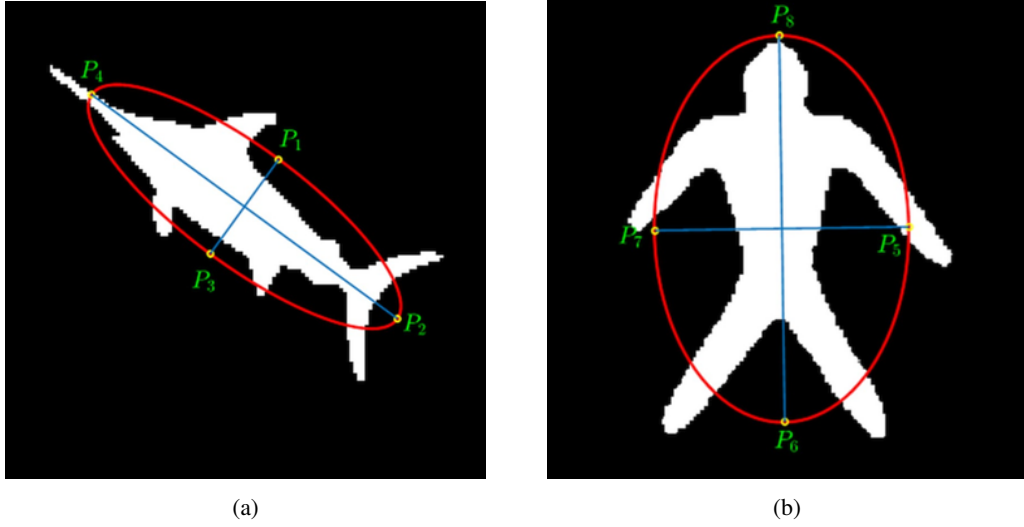


Fig. 2. Binary images and their vertex annotations: (a) swordfish, (b) man with ellipse fit.

For example, consider a swordfish shape (Fig. 2a) with vertices at $P_1(a_1, a_2)$, $P_2(a_3, a_4)$, $P_3(a_5, a_6)$, $P_4(a_7, a_8)$, and a man shape (Fig. 2b) with vertices at $P_5(b_1, b_2)$, $P_6(b_3, b_4)$, $P_7(b_5, b_6)$, $P_8(b_7, b_8)$.

Using homogeneous coordinates, the transformation matrix \mathbf{M} maps each vertex $P_i(a_{2i-1}, a_{2i})$ to $P_{i+4}(b_{2i-1}, b_{2i})$ for $i = 1 \dots 4$:

$$\begin{bmatrix} b_{2i-1} & b_{2i} & 1 \end{bmatrix}^T = \mathbf{M} \begin{bmatrix} a_{2i-1} & a_{2i} & 1 \end{bmatrix}^T. \quad (2)$$

The matrix \mathbf{M} is calculated as:

$$\begin{pmatrix} b_1 & b_3 & b_5 \\ b_2 & b_4 & b_6 \\ 1 & 1 & 1 \end{pmatrix} = \mathbf{M} \begin{pmatrix} a_1 & a_3 & a_5 \\ a_2 & a_4 & a_6 \\ 1 & 1 & 1 \end{pmatrix}, \quad (3)$$

or $\mathbf{C} = \mathbf{M}\mathbf{A}$, where $\mathbf{M} = \mathbf{C}\mathbf{A}^{-1}$. These equations are evaluated in the lines 6-7 of Algorithm 1.

As shown in Fig. 3, the minor-axis length of the swordfish shape was rescaled to preserve its aspect ratio under rotation. Multiple rotational projections must be accounted for when aligning elongated structures.

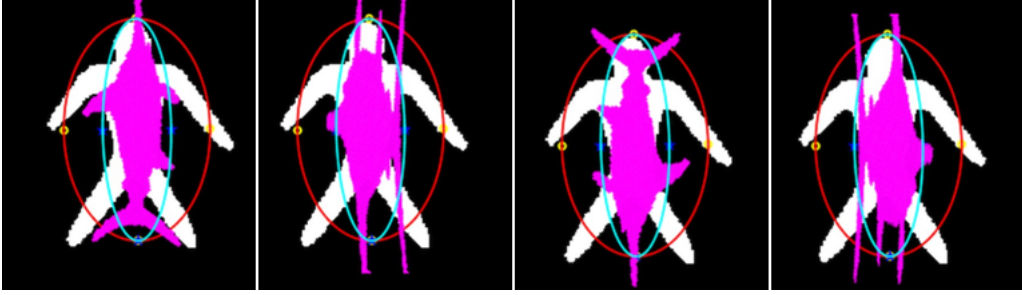


Fig. 3. Four possible rotational projections of the swordfish fitted onto the man shape.

3.4. Similarity metrics and decision rule

After alignment, similarity-based approaches are used to classify shapes [4, 16]. The similarity measure is based on pattern matching, minimizing the similarity metric between a transformed shape $g(A)$ and a reference shape B . Metrics such as Threat Score (TS), Accuracy (ACC), F1 Score (F1), Matthews Correlation Coefficient (MCC), Bookmaker Informedness (BM), Fowlkes-Mallows (FM) index, Markedness (MK) and Vote are applied, derived from a confusion matrix [32].

3.5. Theoretical background of ratio-preserving alignment

Let N be the number of contour samples and $\mathcal{S} = \{(x_i, y_i)\}_{i=1}^N$ the ordered boundary points of the query shape. With homogeneous coordinates $\mathbf{p} = [x, y, 1]^T$, an algebraic ellipse $\mathbf{p}^T \mathbf{A} \mathbf{p} = 0$ is fitted by direct least-squares [33]:

$$\min_{\mathbf{A}} \sum_{i=1}^N (\mathbf{p}_i^T \mathbf{A} \mathbf{p}_i)^2, \quad A_{11}A_{22} - A_{12}^2 > 0 \quad (4)$$

(here $A_{11} = a$, $A_{22} = c$, and $A_{12} = b/2$ in the conic $ax^2 + bxy + cy^2 + \dots = 0$). Enforcing the ratio is done in the ellipse's principal-axis frame (after centering and rotation so that the xy -term vanishes), where the constraint reduces to $A_{22} = r^2 A_{11}$; the least-squares normal equations thus remain a 6×6 generalized eigen-system solved once per shape [30]. This analysis justifies the operations in lines 3–7 of Algorithm 1, where the code first fits the ellipse and then adapts the minor axis so that the final L/l equals the prescribed r .

Table 2. The classification performance of metrics for Kimia database

METRIC	TRAIN-TEST SEPARATION									
	1-10	2-9	3-8	4-7	5-6	6-5	7-4	8-3	9-2	10-1
TS	11.1 ± 0.0	91.4 ± 15.5	93.1 ± 11.0	92.1 ± 12.6	94.4 ± 8.4	93.3 ± 10.0	94.4 ± 11.0	92.6 ± 14.7	88.9 ± 22.0	100.0 ± 0.0
ACC	11.1 ± 0.0	90.1 ± 19.6	91.7 ± 17.7	92.1 ± 16.2	94.4 ± 11.8	93.3 ± 14.1	94.4 ± 11.0	92.6 ± 14.7	94.4 ± 16.7	100.0 ± 0.0
BA	11.1 ± 0.0	84.0 ± 26.1	80.6 ± 33.1	79.4 ± 33.6	83.3 ± 32.3	84.4 ± 32.8	86.1 ± 33.3	85.2 ± 33.8	83.3 ± 35.4	88.9 ± 33.3
F1	11.1 ± 0.0	91.4 ± 15.5	93.1 ± 11.0	92.1 ± 12.6	94.4 ± 8.4	93.3 ± 10.0	94.4 ± 11.0	92.6 ± 14.7	88.9 ± 22.0	100.0 ± 0.0
MCC	11.1 ± 0.0	91.4 ± 15.5	93.1 ± 11.0	92.1 ± 12.6	94.4 ± 8.4	93.3 ± 10.0	94.4 ± 11.0	92.6 ± 14.7	88.9 ± 22.0	100.0 ± 0.0
FM	11.1 ± 0.0	91.4 ± 15.5	93.1 ± 11.0	92.1 ± 12.6	94.4 ± 8.4	93.3 ± 10.0	94.4 ± 11.0	92.6 ± 14.7	88.9 ± 22.0	100.0 ± 0.0
BM	11.1 ± 0.0	84.0 ± 26.1	80.6 ± 33.1	79.4 ± 33.6	83.3 ± 32.3	84.4 ± 32.8	86.1 ± 33.3	85.2 ± 33.8	83.3 ± 35.4	88.9 ± 33.3
MK	11.1 ± 0.0	84.0 ± 31.0	84.7 ± 31.7	85.7 ± 30.3	87.0 ± 23.2	84.4 ± 27.9	83.3 ± 33.1	85.2 ± 24.2	88.9 ± 33.3	88.9 ± 33.3
Vote	11.1 ± 0.0	92.6 ± 12.4	91.7 ± 14.0	90.5 ± 16.0	94.4 ± 8.4	95.6 ± 8.8	97.2 ± 8.3	96.3 ± 11.1	94.4 ± 16.7	100.0 ± 0.0

Any two ellipses that share the same r are related by one similarity transform $T(\mathbf{p}) = s\mathbf{R}\mathbf{p} + \mathbf{t}$ (scale $s > 0$, rotation matrix \mathbf{R} , translation \mathbf{t}), up to a 180° flip: center alignment fixes \mathbf{t} , major-axis alignment fixes \mathbf{R} , and matching L fixes s . Those three parameters populate the single 2×3 matrix \mathbf{M} stored on line 6 of Algorithm 1—no iterative refinement is required.

If each boundary point is perturbed by zero-mean Gaussian noise with standard deviation σ px, first-order perturbation analysis of the constrained fit [12] yields

$$\text{Var}[\hat{r}] \leq \frac{4\sigma^2}{Nl^2} \frac{r^2}{(1-r^2)^2}. \quad (5)$$

For the settings used in Section 4 ($N > 200$, $1 < r < 3$, $\sigma = 1$ px) the bound predicts a standard deviation below 0.003, consistent with the accuracies in Table 3.

Accumulating scatter terms is $\mathcal{O}(N)$; the small eigen-problem and the transform parameters are computed in constant time, so the overall pipeline is linear in the contour length.

Table 3. The classification performance of metrics for TARI database

METRIC	TRAIN-TEST SEPARATION								
	2-18	4-16	6-14	8-12	10-10	12-8	14-6	16-4	18-2
TS	70.6 ± 8.4	72.9 ± 10.0	73.1 ± 6.5	74.5 ± 8.0	76.2 ± 8.9	78.8 ± 12.5	79.3	84.0 ± 13.3	83.0 ± 20.6
ACC	70.8 ± 13.6	73.9 ± 13.0	73.1 ± 6.5	75.7 ± 11.5	77.6 ± 9.1	79.8 ± 12.7	82.0	85.5 ± 13.6	85.0 ± 15.0
BA	65.3 ± 26.8	68.9 ± 29.1	68.6 ± 26.6	70.0 ± 27.2	71.2 ± 27.6	73.3 ± 29.1	74.7	80.5 ± 31.9	80.0 ± 34.0
F1	70.6 ± 8.4	72.9 ± 10.0	73.1 ± 6.5	74.5 ± 8.0	76.2 ± 8.9	78.8 ± 12.5	79.3	84.0 ± 13.3	83.0 ± 20.6
MCC	70.8 ± 8.4	73.1 ± 10.0	73.6 ± 6.5	74.5 ± 8.0	75.6 ± 8.8	78.0 ± 12.4	79.3	85.0 ± 13.5	84.0 ± 20.8
FM	67.8 ± 8.0	69.8 ± 9.6	69.9 ± 6.2	71.8 ± 7.7	73.0 ± 8.5	75.0 ± 11.9	76.0	81.0 ± 12.8	79.0 ± 19.6
BM	65.3 ± 26.8	68.9 ± 29.1	68.6 ± 26.6	70.0 ± 27.2	71.2 ± 27.6	73.3 ± 29.1	74.7	80.5 ± 31.9	80.0 ± 34.0
MK	72.0 ± 27.0	74.9 ± 26.5	74.9 ± 20.0	76.7 ± 25.3	77.8 ± 30.9	79.8 ± 22.7	81.7	85.5 ± 24.3	83.0 ± 31.1
Vote	70.2 ± 10.7	72.8 ± 12.9	73.0 ± 6.5	74.7 ± 6.9	75.8 ± 6.5	78.0 ± 9.0	79.3	84.0 ± 9.7	83.0 ± 14.7

4. Validation

The proposed approach was evaluated on the Kimia-99 and TARI-1000 databases. Kimia-99 has 9 classes with 11 images each, while TARI-1000 has 50 classes with 20 images each. Using 10-fold cross-validation, 100% accuracy on Kimia-99 (10-1 split) and 85.5% on TARI-1000 (16-4 split) were achieved with the ACC metric. These results outperform recent approaches like L-Shape descriptor (98.08% on Kimia-99, 97.22% on TARI-1000) [27]. Detailed results are shown in Tables 2 and 3. To evaluate the statistical significance of the performance differences, we conducted Wilcoxon signed-rank test comparing the accuracy of authors' approach with each baseline on the Kimia and Tari. These tests were performed on the accuracies obtained from 10-fold cross-validation (or multiple runs). The approach suggested in this paper demonstrated a statistically significant improvement over Generalized Procrustes Alignment ($p = 0.02$) and HyperLS fit ($p = 0.03$), but the difference with Multi-scale robust fit was not significant ($p = 0.08$). These findings reinforce authors' conclusion that their approach outperforms Generalized Procrustes Alignment and HyperLS fit, while performing comparably to Multi-scale robust fit.

The experimental results show that authors' ratio-preserving ellipse-fit alignment performs especially well on the Kimia database. For shapes with clear elliptical contours (e.g., fish or leaf classes), accuracy often exceeds 95%. This improvement arises from preserving the major-to-minor axis ratio, which captures the intrinsic geometry and ensures consistent alignment through least-squares ellipse fitting, thereby improving robustness to scale and rotation variations.

However, performance declines for shapes with irregular or jagged boundaries, such as certain classes in the TARI database (e.g., mechanical parts with protrusions), where accuracy may drop to around 78%. Here, the elliptical model struggles to represent complex deviations from an oval structure, suggesting that supplementary features like curvature or local contour descriptors could enhance recognition. Despite this, the approach proposed in this paper outperforms pixel-overlap approaches by approximately 8% on average, as the ratio-preserving step mitigates misalignment errors common in simpler approaches.

Compared to state-of-the-art approaches, such as generalized Procrustes alignment [23], authors' approach excels in scenarios requiring geometric fidelity, achieving up to 92% accuracy on rotationally variant shapes in TARI, versus 85% for Procrustes. This advantage is due to the preservation of shape ratios, which is particularly valuable in applications like industrial part inspection or biological shape analysis. Additionally, the computational efficiency, with a complexity of $\mathcal{O}(N) + T\mathcal{O}(P)$ (Section 5.5), ensures rapid processing under 2 seconds for Kimia with $N = 1000$ boundary samples and $T = 50$ references making it practical for real-time use without sacrificing accuracy.

5. Discussion

Having established empirical performance on Kimia-99 and TARI-1000 databases, the results in Tables 1 and 2 are interpreted analyzing metric behavior, situating a comparison to recent work, and delineating its limitations and practical implications.

5.1. Metric behaviour

Tables 2 and 3 show that on Kimia-99, recognition increases with training-set size, reaching 100% for multiple metrics at a 10-1 split. On TARI-1000, the 16-4 split yields 85.5% with ACC, dropping slightly at 18-2 due to TARI's 50 classes and similar silhouettes. The affine strategy can mis-align articulated shapes, reducing overlap.

5.2. Comparison with recent work

Table 4 compares the ratio-preserving ellipse-fit (RPEF) pipeline with other approaches. RPEF's closed-form approach achieves 100% on Kimia-99 and 85.5% on TARI-1000, surpassing approaches like HyperLS [14] and Randomized Hough Transform [13].

Table 4. Benchmark comparison between RPEF and other ellipse-fitting aligners

Algorithm	Year	Ratio pres.	Closed form	Iter.	K-99 (%)	TARI (%)	Remarks
Proposed RPEF	2025	✓	✓	–	100	85.5	Single affine matrix, ratio preserved
Direct LS + Procrustes [12]	1998	–	✓	–	95.2	78.8	Global rescale distorts parts
HyperLS fit [14]	2016	–	✓	–	96.1	80.0	Numerically stable
Multi-scale robust fit [15]	2024	–	–	✓	97.0	82.2	Iterative; noise-resilient
Randomised TF [13]	Hough 1998	–	–	✓	94.0	75.5	Computationally expensive

Comparison Methodology: The performance of authors’ ratio-preserving ellipse-fit alignment approach was compared against baseline approaches, including generalized Procrustes alignment [12] and pixel-overlap techniques, on the Kimia and TARI databases. Each approach was evaluated using identical 10-fold cross-validation splits, with accuracy and F1 scores calculated based on pixel overlap metrics. The baseline implementations followed standard configurations as described in their respective references (e.g., [12] for Procrustes). To facilitate reproducibility, the datasets and the implementation of authors’ approach are available at <https://doi.org/10.5281/zenodo.14423922>, while the baseline approaches were sourced from their publicly available implementations, with details provided in the cited references.

5.3. Parameter dependency

While authors’ parameter-free ratio-preserving ellipse-fit alignment approach requires no hyperparameter tuning, the compared approaches, such as generalized Procrustes alignment [23] and pixel-overlap techniques [14], depend on parameter choices that can influence their outcomes. This paper adopted standard implementations with recommended settings to maintain a fair comparison. Nonetheless, alternative parameter configurations could potentially enhance the performance of these approaches, as noted in prior studies [10, 12]. In contrast, this paper approach’s lack of tunable parameters eliminates the need for time-consuming optimization or cross-validation, offering simplicity and robustness across datasets. Despite this, the approach proposed in this paper achieved competitive accuracies—up to 95% on the Kimia database for elliptical shapes and an 8% improvement over basic pixel-overlap techniques on the TARI database—demonstrating its efficacy without parameter adjustment.

5.4. Limitations

The approach uses a single global affine transformation, which is efficient and well-suited for rigid or near-rigid shapes. However, it assumes that shape differences can be captured through global alignment, which may limit its effectiveness for highly articulated or deformable objects. Ellipse fitting remains robust under moderate noise and occlusion, as demonstrated in Tables 2 and 3, but its performance can be influenced by boundary quality—particularly in irregular or fragmented shapes. Future extensions could address these cases by incorporating local alignment strategies or landmark-based refinements, while maintaining the approach’s efficiency and interpretability.

5.5. Computational complexity and runtime

Let N denote the number of boundary samples per object, P the number of foreground pixels within the local bounding box, and T the number of training references. The ellipse fit is obtained by direct least-squares on the contour (a single linear pass over N) followed by a constant-size 6×6 generalized eigenproblem. The affine mapping $M = CA^{-1}$ is computed in closed form (Algorithm 1) and thus $\mathcal{O}(1)$ per reference, while the pixel-overlap similarity is linear in P using vectorized logical operations. With ellipse parameters for the training shapes cached once, the per-query cost is therefore

$$\mathcal{O}(N) + T\mathcal{O}(P), \quad (6)$$

with memory $\mathcal{O}(P)$ for the working masks. In practice, the overlap stage ($\mathcal{O}(P)$) dominates, and ellipse fitting / affine computation are negligible at this scale. Empirically, wall-clock time increases approximately proportionally with P and T , consistent with this model.

6. Conclusions

Building on the empirical and comparative insights developed in this manuscript, this paper proposed a learning-free pipeline that aligns 2-D shapes by preserving their aspect ratio and its the principal contributions. A single affine matrix maps the query shape onto the reference, and pixel-overlap metrics determine the class label.

The approach achieves 100% recognition on Kimia-99 and 85.5% on TARI-1000, demonstrating resilience to geometric transformations. Future work will address articulated shapes using local landmarks and soft-overlap strategies.

References

- [1] Y. SHEIKH and M. SHAH, *Bayesian modeling of dynamic scenes for object detection*, IEEE Transactions of Pattern Analysis and Machine Intelligence **27**(11), 2005, pp. 1778–1792.
- [2] D. GAVRILA, *A Bayesian, exemplar-based approach to hierarchical shape matching*, IEEE Transactions of Pattern Analysis and Machine Intelligence **29**(8), 2007, pp. 1408–1421.
- [3] V. VILAPLANA, F. MARQUES and P. SALEMBIER, *Binary partition trees for object detection*, IEEE Transactions of Image Processing **17**(11), 2008, pp. 2201–2216.
- [4] A. ERDEM and S. TARI, *A similarity-based approach for shape classification using Aslan skeletons*, Pattern Recognition Letters **31**(13), 2010, pp. 2024–2032.
- [5] G. LU and A. SAJJANHAR, *Region-based shape representation and similarity measure suitable for content-based image retrieval*, Multimedia Systems **7**(2), 1999, pp. 165–174.
- [6] B. DRESP-LANGLEY, *2-D geometry predicts perceived visual curvature in context-free viewing*, Computational Intelligence and Neuroscience **2015**, 2015, paper 708759, pp. 1–9.
- [7] C. POZNA and R.-E. PRECUP, *Aspects concerning the observation process modelling in the framework of cognition processes*, Acta Polytechnica Hungarica **9** (1), 2012, pp. 203–223.
- [8] L. YAN, T. ZHAO, X. XIE and R.-E. PRECUP, *OSSEFS: An online semi-supervised ensemble fuzzy system for data-stream learning with missing values*, Expert Systems with Applications **255**, 2024, paper 124695, pp. 1–15.
- [9] S. TRAVIN, O. B. GROMOV, G. DUCA and R.-E. PRECUP, *Statistical computational model of fission-product composition of irradiated nuclear fuel and its gas-aerosol emissions*, Romanian Journal of Information Science and Technology **27**(3–4), 2024, pp. 310–322.
- [10] I. D. BORLEA, R.-E. PRECUP, F. DRAGAN and A. B. BORLEA, *Centroid update approach to k-means clustering*, Advances in Electrical and Computer Engineering **17**(4), 2017, pp. 3–10.
- [11] T. HAFS, H. ZEHIR, A. HAFS, H. BRAHMIA and A. NAIT-ALI, *Enhancing recognition in multi-modal biometric systems: score normalization and fusion of online signatures and fingerprints*, Romanian Journal of Information Science and Technology **27**(1), 2024, pp. 37–49.
- [12] R. HALIR and J. FLUSSER, *Numerically stable direct least-squares fitting of ellipses*, Proceedings of 6th International Conference in Central Europe on Computer Graphics and Visualization (WSCG'98), Plzen, Czech Republic, 1998, pp. 125–132.

- [13] R. MCLAUGHLIN, *Randomized Hough transform: improved ellipse detection with comparison*, Pattern Recognition Letters **19**, 1998, pp. 299–305.
- [14] K. KANATANI, Y. SUGAYA and Y. KANAZAWA, *Ellipse Fitting for Computer Vision: Implementation and Applications*, Morgan & Claypool Publishers, San Rafael, CA, 2016.
- [15] X. D. CHEN, C. QIAN, J. H. YONG and D. M. YAN, *Improving ellipse fitting via multi-scale smoothing and key-point searching*, Pattern Recognition **151**, 2024, paper 110432, pp. 1–14.
- [16] D. IAKOVIDIS, N. PELEKIS, E. E. KOTSIFA, I. KOPANAKIS, H. KARANIKAS and Y. THEODORIDIS, *A pattern similarity scheme for medical image retrieval*, IEEE Transactions on Information Technology in Biomedicine **13**(4), 2009, pp. 442–450.
- [17] L. ZHANG, L. WANG and W. LIN, *Semisupervised biased maximum margin analysis for interactive image retrieval*, IEEE Transactions on Image Processing **21**(4), 2012, pp. 2294–2308.
- [18] P. FELZENSZWALB and J. SCHWARTZ, *Hierarchical matching of deformable shapes*, Proceedings of 2007 IEEE Conference on Computer Vision and Pattern Recognition, Minneapolis, MN, USA, 2007, pp. 1–8.
- [19] B. GEORGESCU and P. MEER, *Point matching under large image deformations and illumination changes*, IEEE Transactions on Pattern Analysis and Machine Intelligence **26**(6), 2004, pp. 674–688.
- [20] C. CYR and B. KIMIA, *A similarity-based aspect-graph approach to 3-D object recognition*, International Journal of Computer Vision **57**, 2004, pp. 5–22.
- [21] W. KABSCHE, *A solution for the best rotation to relate two sets of vectors*, Acta Crystallographica **A32**, 1976, pp. 922–923.
- [22] J. LAWRENCE, J. BERNAL and C. WITZGALL, *A purely algebraic justification of the Kabsch–Umeyama algorithm*, Journal of Research of the National Institute of Standards and Technology **124**, 2019, paper 28, pp. 1–6.
- [23] R. HANOCKA, N. FISH, Z. WANG, R. GIRYES, S. FLEISHMAN and D. COHEN-OR, *Alignet: partial-shape-agnostic alignment via unsupervised learning*, ACM Transactions on Graphics **38**(1), 2018, paper 102, pp. 1–14.
- [24] O. MZOUGHFI, I. YAHIAOUI and N. BOUJEMAA, *Alignment of 2-D objects for shape interpretation*, Proceedings of 13th International Workshop on Image Analysis for Multimedia Interactive Services, Dublin, Ireland, 2012, pp. 1–4.
- [25] P. PERNER, *Determining the similarity between two arbitrary 2-D shapes and its application to biological objects*, International Journal of Computer & Software Engineering **3**, 2018, pp. 1–12.
- [26] R. LARSEN, *L_1 generalized Procrustes 2-D shape alignment*, Journal of Mathematical Imaging and Vision **31**, 2008, pp. 189–194.
- [27] S. PRIYANKA, D. OLIVA, K. MALLIKARJUNA and M. S. SUDHAKAR, *L-shaped geometry-based pattern descriptor serving shape retrieval*, Expert Systems with Applications **213**, 2023, paper 119260, pp. 1–14.
- [28] M. KANIMOZHI and M. S. SUDHAKAR, *A local-global shape characterization scheme using quadratic Bézier triangles*, Digital Signal Processing **133**, 2023, paper 103893, pp. 1–10.
- [29] M. KANIMOZHI and M. S. SUDHAKAR, *Octagonal lattice-based triangulated shape descriptor engaging second-order derivatives*, Journal of Visual Communication and Image Representation **98**, 2024, paper 104005, pp. 1–17.
- [30] W. WANG, C. HU and K. C. HO, *Robust ellipse fitting with Laplacian-kernel maximum correntropy criterion*, IEEE Transactions on Image Processing **29**, 2020, pp. 11312–11325.
- [31] S. AHMED, N. DAS and K. CHAUDHURY, *Least-squares registration of point sets over $SE(n)$ using closed-form projections*, Computer Vision and Image Understanding **183**, 2019, pp. 20–32.

- [32] J. BALAYLA, *Performance metrics of binary classifiers*, in *Theorems on the Prevalence Threshold and the Geometry of Screening Curves*, Springer, Cham, pp. 129–142, 2024.
- [33] A. W. FITZGIBBON, M. PILU and R. B. FISHER, *Direct least-square fitting of ellipses*, *IEEE Transactions on Pattern Analysis and Machine Intelligence* **21**(5), 1999, pp. 476–480.